Extended Derivations and Additional Simulations for Aerial Robots Tethered by Cables or Bars

Online appendix to:
"Dynamics, Control and Estimation for Aerial Robots Tethered by Cables or Bars"
IEEE Transaction on Robotics

Marco Tognon[1] and Antonio Franchi[1]

I. Introduction

This document is a technical attachment to [1] as an extension of the differential flatness and simulation sections.

The reader interested in the analysis and control of tethered aerial vehicles is also referred to [1], where flatness, controllability and observability is studied, to [2] where the case of a moving base is thoroughly analyzed, to [3] where real experiments for tethered landing on sloped surfaces is shown, and to [4], [5] where the case of multiple tethered vehicles is investigated.

A. Aerial physical interaction

Tethered aerial vehicles constitute an example of aerial vehicles physically interacting with the external environment. For the reader interested in this rapidly expanding and broad topic we also suggest the reading of [6], where a force nonlinear observer for aerial vehicles is proposed, of [7], where an IDA-PBC controller is used for modulating the physical interaction of aerial robots, of [8], [9] where fully actuated platforms for full wrench exertion are presented, of [10]–[12] where the capabilities of exerting forces with a tool are studied, and finally of [13]–[15] where aerial manipulators with elastic-joint arms are modeled and their controllability properties discovered.

II. Detailed Differential Flatness Derivation

In this section we provide a more detailed and step-by-step derivation of the proof of the flatness property of the system.

A. Flatness with Respect to $\mathbf{y}^a$

From the definition of $\mathbf{y}^a$ we directly have that $\mathbf{x} = \begin{bmatrix} y_1^a & \dot{y}_1^a & y_2^a & \dot{y}_2^a \end{bmatrix}^T$. Then, inverting the equations:

$$\begin{aligned} \dot{x}_1 &= a_1 c_{x_1} + a_2 c_{x_1+x_3} u_1 \\ \dot{x}_4 &= a_4 u_2, \end{aligned} \tag{1}$$

we can write the inputs as a function of the output and some of its derivatives

$$\begin{aligned} u_1 &= \frac{\dot{x}_2 - a_1 c_{x_1}}{a_2 c_{x_1+x_3}} = \frac{\ddot{y}_1^a - a_1 c_{y_1^a}}{a_2 c_{y_1^a + y_2^a}} = u_1(y_1^a, \dot{y}_1^a, \ddot{y}_1^a, y_2^a) \\ u_2 &= \dot{x}_4 / a_3 = \ddot{y}_2^a / a_3 = u_2(\ddot{y}_2^a). \end{aligned}$$

B. Flatness with Respect to $\mathbf{y}^b$

First of all we have directly $x_1 = \varphi = y_1^b$ and $x_2 = \dot{\varphi} = \dot{y}_1^b$. Then let us define

$$\mathbf{r} = -m_R \ddot{\mathbf{p}}_B(y_1^b, \dot{y}_1^b, \ddot{y}_1^b, y_2^b) - y_2^b \mathbf{d}(y_1^b) - m_R g \mathbf{z}_W,$$

that depends only on $y_1^b, \dot{y}_1^b, \ddot{y}_1^b, y_2^b$ and some constant parameters of the system since

$$\ddot{\mathbf{p}}_B = -l\mathbf{d}\dot{\varphi}^2 + l\mathbf{d}^\perp \ddot{\varphi} = \ddot{\mathbf{p}}_B(y_1^b, \dot{y}_1^b, \ddot{y}_1^b, y_2^b).$$

Then, using the force balance equation, i.e.,

$$m_R \ddot{\mathbf{p}}_B = m_R(-l\mathbf{d}\dot{\varphi}^2 + l\mathbf{d}^\perp \ddot{\varphi}) = -f_L \mathbf{d} - f_R \mathbf{z}_B - m_R g \mathbf{z}_W,$$

we get

$$f_R \mathbf{z}_B = u_1 \mathbf{z}_B = u_1 [-s_{x_3} \ 0 \ -c_{x_3}]^T = \mathbf{r}(y_1^b, \dot{y}_1^b, \ddot{y}_1^b, y_2^b), \tag{2}$$

where $\mathbf{r}(\cdot,\cdot,\cdot,\cdot) = [r_1 \ r_2 \ r_3]^T$ represents the function from $\mathbb{R}^2 \times \mathbb{R}^2 \times \mathbb{R}^2 \times \mathbb{R}^2$ to $\mathbb{R}^3$. If $\|\mathbf{r}\| \neq 0$, from (2) we can retrieve u_1 and x_3 as

$$\begin{aligned} u_1 &= \|\mathbf{r}\| = u_1(y_1^b, \dot{y}_1^b, \ddot{y}_1^b, y_2^b) \\ x_3 &= \text{atan2}\,(r_1/\|\mathbf{r}\|, r_3/\|\mathbf{r}\|) = x_3(y_1^b, \dot{y}_1^b, \ddot{y}_1^b, y_2^b). \end{aligned} \tag{3}$$

Differentiating x_3 w.r.t. time we obtain x_4

$$\begin{aligned} x_4 &= \frac{d}{dt} x_3(y_1^b, \dot{y}_1^b, \ddot{y}_1^b, y_2^b) \\ &= \frac{r_{3n}\dot{r}_{1n} - r_{1n}\dot{r}_{3n}}{r_{1n}^2 + r_{3n}^2} \\ &= x_4(y_1^b, \dot{y}_1^b, \ddot{y}_1^b, y_1^{b(3)}, y_2^b, \dot{y}_2^b), \end{aligned}$$

where we have defined $r_{1n} = r_1/\|\mathbf{r}\|$ and $r_{3n} = r_3/\|\mathbf{r}\|$. Further differentiating x_4 and using (1) we finally obtain u_2

$$u_2 = J_R \frac{d}{dt} x_4(y_1^b, \ldots, y_1^{b(3)}, y_2^b, \dot{y}_2^b) = u_2(y_1^b, \ldots, y_1^{b(4)}, y_2^b, \dot{y}_2^b, \ddot{y}_2^b).$$

[1]LAAS-CNRS, Université de Toulouse, CNRS, Toulouse, France, marco.tognon@laas.fr, antonio.franchi@laas.fr

This work has been partially funded by the European Union's Horizon 2020 research and innovation programme under grant agreement No 644271 AEROARMS.

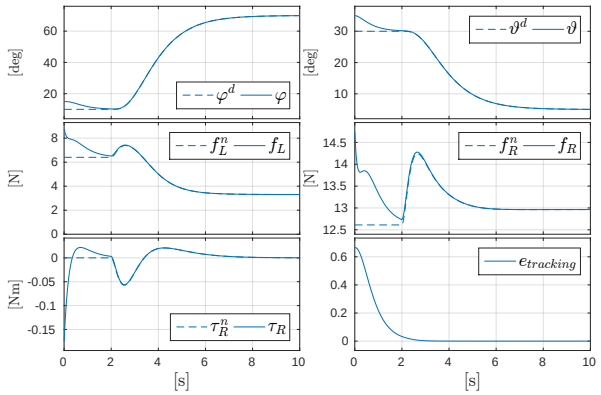

(a) Controller Results.

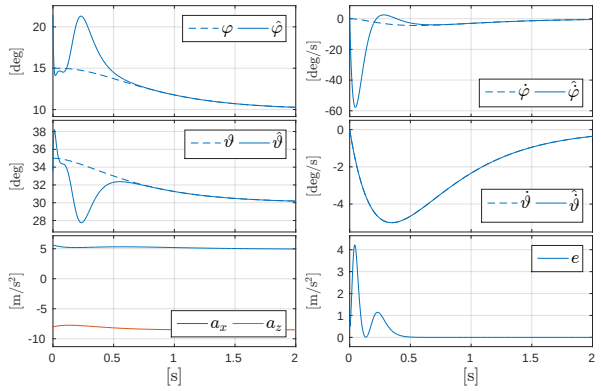

(b) Observer Results: Only the first two seconds are shown since after this time the estimation follows the state with high fidelity for all the rest of the simulation.

Fig. 1: Controller $\Gamma^{a'}$ with initial tracking and estimation error. In this plot and in the following the superscript $\cdot^n$ represents the nominal state and inputs, computed thanks to the differential flatness, needed to track the desired trajectories.

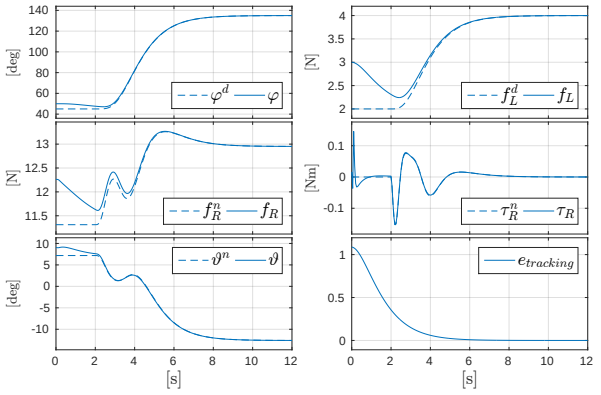

(a) Controller Results.

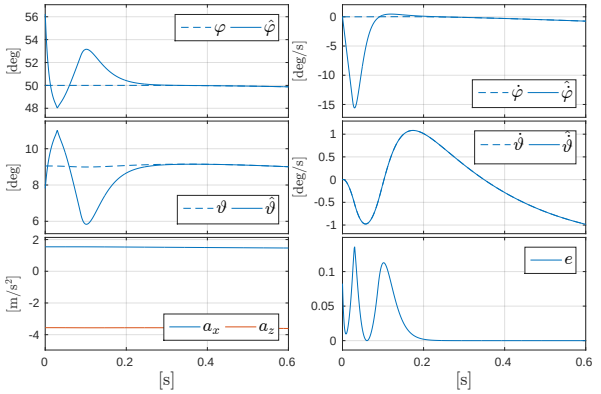

(b) Observer Results: Only the first 0.6 seconds are shown since after this time the estimation follows the state with high fidelity for all the rest of the simulation.

Fig. 2: Controller Γ^b with initial tracking and estimation error.

III. Additional Simulations

Within this section we shall provide some additional results obtained by simulations in order to prove the validity of the proposed method.

Regarding the parameters of the system we used the same values presented in Sec. VI of [1]. Analogously for the desired trajectories. To have a more complete validation, in the following we show the results of the convergence and robustness of the proposed method under different non ideal conditions, such as: a) initial tracking and estimation error, b) parametric variations, c) noisy sensor measurements, and d) motor time constant.

A. Initial errors

In this section we want to show the closed loop stability of the system in dynamic condition even with some initial tracking and estimation error. In Fig. 1 and Fig. 2, one can see that after the convergence of the observer, taking less than one second, both controllers $\Gamma^{a'}$ and Γ^b exponentially steer the outputs along the desired trajectories.

B. Parametric variations

The purpose of the next sections is to investigate the robustness of the proposed methods. In particular we consider some parameter variation between the real model and controller/observer. Indeed in a real scenario we can not know exactly each parameter of the system, thus the controller and observer would be based on some nominal parameter values different from the real one.

Fig. 3 and Fig. 4 show the performances of the controller $\Gamma^{a'}$ and Γ^b with a relative variation of 0.05 for each parameter (Δm_R, Δl and ΔJ_R). We can notice that due to the uncertainty of the model we have some nonzero errors in the tracking and on the estimation of the state. Nevertheless the system remains stable and the tracking and estimation errors result bounded. In principle an integrator term in the controller could overcome the constant steady state error, thought the control action is computed from an estimation of actual output based on the input and on the estimation of the state. The last one does not converge to the real one since the observer has a steady state error and so also the estimation of the output.

The addition of an integrator term in the controller does not imply an improvement of the performances since the observer output has a bias due to the estimation error. On the contrary, in the case the feedback control could be done

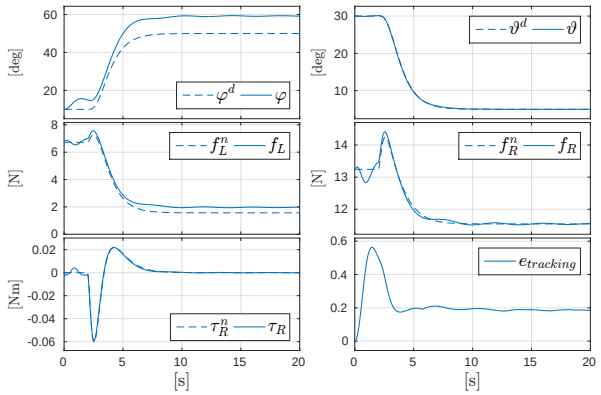

(a) Controller Results.

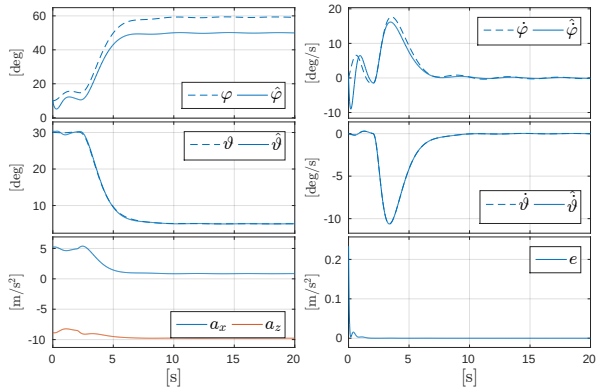

(b) Observer Results.

Fig. 3: Controller $\Gamma^{a'}$: possible real parametric variation with a relative variation of 0.05 (i.e., 5%) for each parameter.

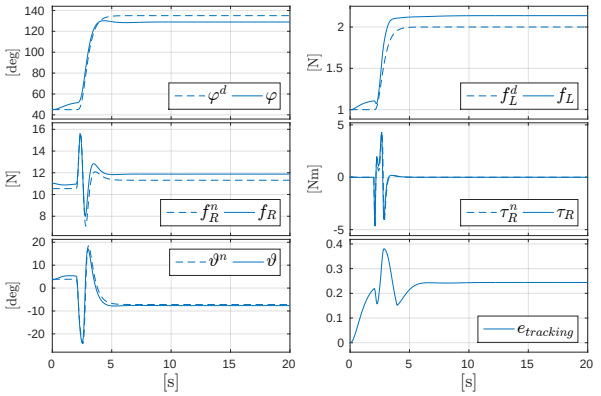

(a) Controller Results.

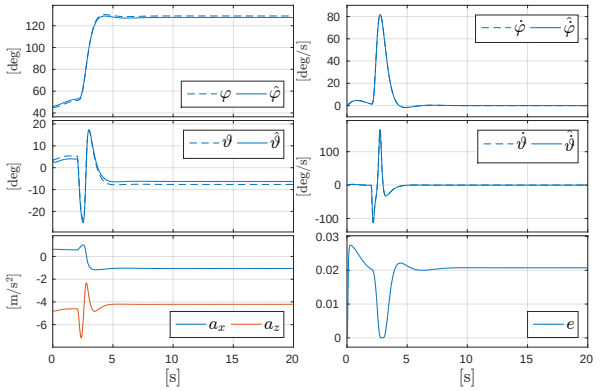

(b) Observer Results.

Fig. 4: Controller Γ^{b}: possible real parametric variation with a relative variation of 0.05 (i.e., 5%) for each parameter.

based on the real outputs, then the integrator term would solve the steady state error due to the parameter variations. Indeed, in Fig. 5, where the performances are showed in the case that the real output is assumed measured and an integrator term is added on the controller, one can observe that the mean tracking error reduces a lot, especially in the steady state phase.

C. Noise on the Measurements

In this last section we investigate the robustness of the proposed method with the presence of noise in the measurements. We considered the accelerometer and the gyroscope with white noise component of variance $0.1[\mathrm{m/s^2}]$ and $0.01[\mathrm{rad/s}]$, respectively, that correspond to typical values of real sensors.

From Fig. 6, for the controller $\Gamma^{a'}$, we can observe that the estimated state shows some noise but the corresponding error remains always limited. Due to the noisy component on the estimated state the control action presents some oscillations that imply a non exact tracking of the desired trajectory. Nevertheless the tracking error remains small and always bounded. To achieve these results we had to reduce the gains of both controller and observer. Indeed, high gain values increase the convergence speed but also the negative effects of the noisy measurements. In general the two controllers $\Gamma^{a'}$ and Γ^{b} do not show particular different behaviors.

D. Motors Time Constant

In a real scenario, one motor can not instantaneously change the spinning velocity of the propeller, and in turn the thrust produced. Indeed, this discontinuous variation of the speed would require the application of an infinite torque by the motor, that is clearly not possible. Instead the dynamics of the motor is characterized by a certain time constant, $\tau_M \in \mathbb{R}$, that quantifies the time needed to change the motor speed. In this section we analyze this additional non ideality testing the proposed method with different non ideal motors characterized by an increasing time constant. In Fig. 7 we show the relative mean and variance of the tracking error for the different time constant values τ_M. The plots clearly shows that increasing the time constant the tracking error increases as well, especially during the dynamic part of the desired trajectory (Phase 2). Indeed, for motors with higher time constant, the error between commanded and actuated thrust on each propeller increases causing a bigger tracking error.

This analysis is important for the scalability of the system. Indeed, bigger vehicles with higher mass imply the need of an higher lift that can be in general generated by bigger propellers. This in turn requires the use of bigger motors that are characterized by an larger time constant. Finally, as shown in Fig 7, the larger mass of the system and the

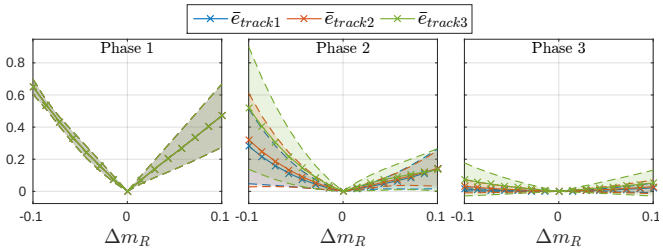

(a) Variation on m_R.

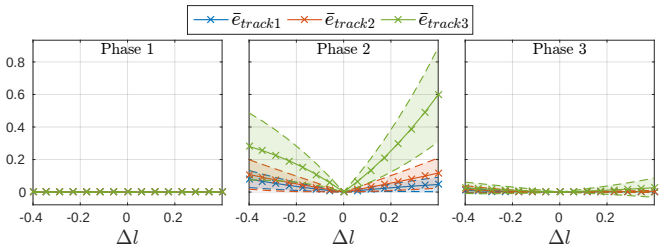

(b) Variation on l.

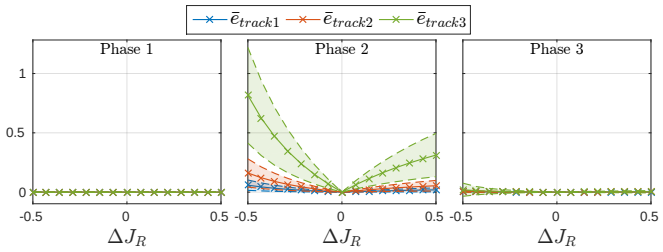

(c) Variation on J_R.

Fig. 5: Parametric variation - Controller Γ^b with real output and an integrator term. The subscript 1,2, and 3 corresponds to the three different trajectory times: 1) 7[s], 2) 5[s] and 3) 3[s], respectively. Over the displayed range of parametric variation the performances are very bad or the system results to be even unstable.

larger time constant of the motors reduce the agility of the system. Therefore, when we increase the dimensions and the mass of the vehicle, in order to still obtain good tracking performances, it is necessary to reduce the agility of the desired maneuver reducing the demanded accelerations.

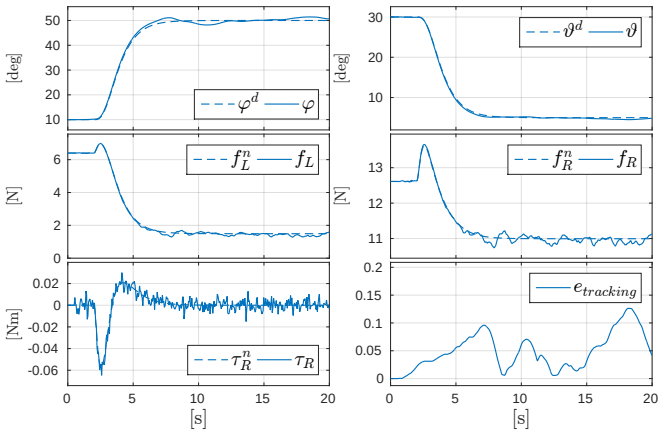

(a) Controller Results.

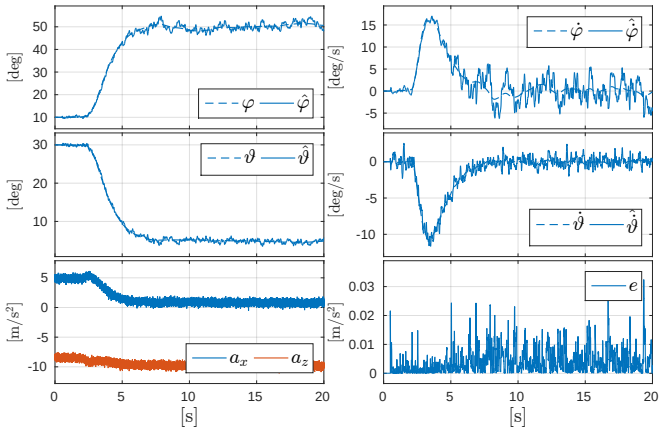

(b) Observer Results.

Fig. 6: Controller $\Gamma^{a'}$: Noisy measurements.

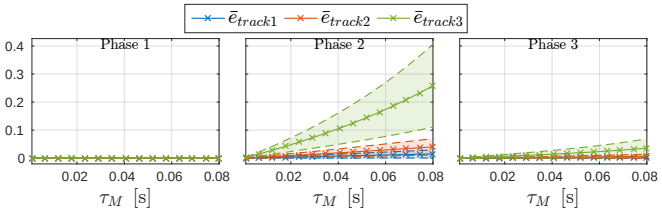

Fig. 7: *Motor time constant - Controller* Γ^b *(elevation and link force).*

REFERENCES

[1] M. Tognon and A. Franchi, "Dynamics, control and estimation for aerial robots tethered by cables or bars," *IEEE Trans. on Robotics*, 2017.

[2] M. Tognon, S. S. Dash, and A. Franchi, "Observer-based control of position and tension for an aerial robot tethered to a moving platform," *IEEE Robotics and Automation Letters*, vol. 1, no. 2, pp. 732–737, 2016.

[3] M. Tognon, A. Testa, E. Rossi, and A. Franchi, "Takeoff and landing on slopes via inclined hovering with a tethered aerial robot," in *2016 IEEE/RSJ Int. Conf. on Intelligent Robots and Systems*, Daejeon, South Korea, Oct. 2016.

[4] M. Tognon and A. Franchi, "Control of motion and internal stresses for a chain of two underactuated aerial robots," in *14th European Control Conference*, Linz, Austria, Jul. 2015, pp. 1614–1619.

[5] ——, "Nonlinear observer for the control of bi-tethered multi aerial robots," in *2015 IEEE/RSJ Int. Conf. on Intelligent Robots and Systems*, Hamburg, Germany, Sep. 2015, pp. 1852–1857.

[6] B. Yüksel, C. Secchi, H. H. Bülthoff, and A. Franchi, "A nonlinear force observer for quadrotors and application to physical interactive tasks," in *2014 IEEE/ASME Int. Conf. on Advanced Intelligent Mechatronics*, Besançon, France, Jul. 2014, pp. 433–440.

[7] ——, "Reshaping the physical properties of a quadrotor through IDA-PBC and its application to aerial physical interaction," in *2014 IEEE Int. Conf. on Robotics and Automation*, Hong Kong, China, May. 2014, pp. 6258–6265.

[8] S. Rajappa, M. Ryll, H. H. Bülthoff, and A. Franchi, "Modeling, control and design optimization for a fully-actuated hexarotor aerial vehicle with tilted propellers," in *2015 IEEE Int. Conf. on Robotics and Automation*, Seattle, WA, May 2015, pp. 4006–4013.

[9] M. Ryll, D. Bicego, and A. Franchi, "Modeling and control of FAST-Hex: a fully-actuated by synchronized-tilting hexarotor," in *2016 IEEE/RSJ Int. Conf. on Intelligent Robots and Systems*, Daejeon, South Korea, Oct. 2016.

[10] M. Mohammadi, A. Franchi, D. Barcelli, and D. Prattichizzo, "Cooperative aerial tele-manipulation with haptic feedback," in *2016 IEEE/RSJ Int. Conf. on Intelligent Robots and Systems*, Daejeon, South Korea, Oct. 2016.

[11] G. Gioioso, A. Franchi, G. Salvietti, S. Scheggi, and D. Prattichizzo, "The Flying Hand: a formation of uavs for cooperative aerial tele-manipulation," in *2014 IEEE Int. Conf. on Robotics and Automation*, Hong Kong, China, May. 2014, pp. 4335–4341.

[12] G. Gioioso, M. Mohammadi, A. Franchi, and D. Prattichizzo, "A force-based bilateral teleoperation framework for aerial robots in contact with the environment," in *2015 IEEE Int. Conf. on Robotics and Automation*, Seattle, WA, May 2015, pp. 318–324.

[13] B. Yüksel, N. Staub, and A. Franchi, "Aerial robots with rigid/elastic-joint arms: Single-joint controllability study and preliminary experiments," in *2016 IEEE/RSJ Int. Conf. on Intelligent Robots and Systems*, Daejeon, South Korea, Oct. 2016.

[14] B. Yüksel, G. Buondonno, and A. Franchi, "Differential flatness and control of protocentric aerial manipulators with any number of arms and mixed rigid-/elastic-joints," in *2016 IEEE/RSJ Int. Conf. on Intelligent Robots and Systems*, Daejeon, South Korea, Oct. 2016.

[15] B. Yüksel, S. Mahboubi, C. Secchi, H. H. Bülthoff, and A. Franchi, "Design, identification and experimental testing of a light-weight flexible-joint arm for aerial physical interaction," in *2015 IEEE Int. Conf. on Robotics and Automation*, Seattle, WA, May 2015, pp. 870–876.